NPIP: A skew line needle configuration optimization system for HDR brachytherapy

Timmy Siauw[a)]
Department of Civil and Environmental Engineering, University of California, Berkeley, 760 Davis Hall, Berkeley, California 94720-1710

Adam Cunha
Department of Radiation Oncology, University of California, San Francisco, Comprehensive Cancer Center, 1600 Divisadero Street, Suite H1031, San Francisco, California 94143-1708

Dmitry Berenson
Department of Electrical Engineering and Computer Science, University of California, Berkeley, 4th Floor Sutardja Dai Hall, Berkeley, California 94720-1764

Alper Atamtürk
Department of Industrial Engineering and Operations, University of California, Berkeley, 4141 Etcheverry Hall, Berkeley, California 94720-1777

I-Chow Hsu
Department of Radiation Oncology, University of California, San Francisco, Comprehensive Cancer Center, 1600 Divisadero Street, Suite H1031, San Francisco, California 94143-1708

Ken Goldberg
Department of Industrial Engineering and Operations Research and Department of Electrical Engineering and Computer Science, University of California, Berkeley, 4141 Etcheverry Hall, Berkeley, California 94720-1777

Jean Pouliot
Department of Radiation Oncology, University of California, San Francisco, Comprehensive Cancer Center, 1600 Divisadero Street, Suite H1031, San Francisco, California 94143-1708

(Received 17 February 2012; revised 22 May 2012; accepted for publication 23 May 2012; published 27 June 2012)

Purpose: In this study, the authors introduce skew line needle configurations for high dose rate (HDR) brachytherapy and needle planning by integer program (NPIP), a computational method for generating these configurations. NPIP generates needle configurations that are specific to the anatomy of the patient, avoid critical structures near the penile bulb and other healthy structures, and avoid needle collisions inside the body.

Methods: NPIP consisted of three major components: a method for generating a set of candidate needles, a needle selection component that chose a candidate needle subset to be inserted, and a dose planner for verifying that the final needle configuration could meet dose objectives. NPIP was used to compute needle configurations for prostate cancer data sets from patients previously treated at our clinic. NPIP took two user-parameters: a number of candidate needles, and needle coverage radius, δ. The candidate needle set consisted of 5000 needles, and a range of δ values was used to compute different needle configurations for each patient. Dose plans were computed for each needle configuration. The number of needles generated and dosimetry were analyzed and compared to the physician implant.

Results: NPIP computed at least one needle configuration for every patient that met dose objectives, avoided healthy structures and needle collisions, and used as many or fewer needles than standard practice. These needle configurations corresponded to a narrow range of δ values, which could be used as default values if this system is used in practice. The average end-to-end runtime for this implementation of NPIP was 286 s, but there was a wide variation from case to case.

Conclusions: The authors have shown that NPIP can automatically generate skew line needle configurations with the aforementioned properties, and that given the correct input parameters, NPIP can generate needle configurations which meet dose objectives and use as many or fewer needles than the current HDR brachytherapy workflow. Combined with robot assisted brachytherapy, this system has the potential to reduce side effects associated with treatment. A physical trial should be done to test the implant feasibility of NPIP needle configurations. [http://dx.doi.org/10.1118/1.4728226]

Key words: NPIP, optimization, HDR brachytherapy, needle planning, integer program

I. INTRODUCTION

Prostate high dose rate (HDR) brachytherapy has an excellent survival and local control rate.[1] However, treatment quality can be improved by reducing side effects.[2,3] For example, erectile dysfunction is a side effect that may be caused by trauma to the cavernous arteries running along the side of the penile bulb.[4–6] One way to reduce the rate of erectile dysfunction may be through computer-generated needle configurations that avoid these organ structures. There are also other benefits to the careful planning of HDR brachytherapy needle configurations, or needle planning. For example, needle planning will be a critical component of using robot needle insertion devices to assist physicians in brachytherapy.

The standard clinical workflow for HDR brachytherapy uses a fixed rigid template to help physicians insert needles. Templates allow needles to be accurately inserted to a desired location but restrict the needle trajectories to a parallel geometry. As a result, puncturing healthy structures such as the penile bulb is sometimes unavoidable.

Recently, a few clinics have developed freehand, ultrasound-guided, temporary prostate implant techniques.[7] These nontemplate-based techniques are designed to be used in a clinical environment with image-guidance, remote afterloading, and computerized dwell time anatomy-based optimization. Freehand techniques give physicians increased freedom to place needles and avoid healthy structures. However, inserting needles by freehand is more difficult to execute than using a template and requires proficiency in ultrasonography and needle insertion based on ultrasound images.

The placement difficulties associated with freehand implant techniques can be addressed through robotics. Robots can assist physicians in guiding needles or insert needles autonomously along nonparallel trajectories to a target point. However in prostate HDR brachytherapy, the positioning of needles is critical for achieving clinical dose objectives. Recent work has shown that nonparallel needle configurations are capable of both achieving dose objectives and avoiding critical structures near the penile bulb.[8] However, these configurations had to be designed manually, which is impractical in a clinical setting. To incorporate robots into the clinic, a needle configuration planning method is required that is automatic and utilizes all the degrees of freedom of needle insertion robots.

In this study, needle planning for HDR brachytherapy is explored. Needle configurations are modeled as arrangements of skew line segments (i.e., nonparallel, nonintersecting lines). An automated needle planning system is presented for generating skew line needle configurations for HDR brachytherapy which are specific to the anatomy of the patient and avoid healthy structures—in particular critical structures near the penile bulb. It is shown that given the correct input parameters, this system can generate needle configurations which meet clinical dose objectives and use as many or fewer needles than the current HDR brachytherapy workflow.

Figure 1 shows a patient anatomy set with an actual 16-needle implant (left), and a 13-needle skew line needle configuration computed using our system (right). The actual implant intersected the penile bulb six times, while the computed needle configuration did not intersect the bulb. All clinical dose objectives for the patient were met using both needle configurations. In the future this system, or one like it, will be critical for bringing robots into the brachytherapy clinic.

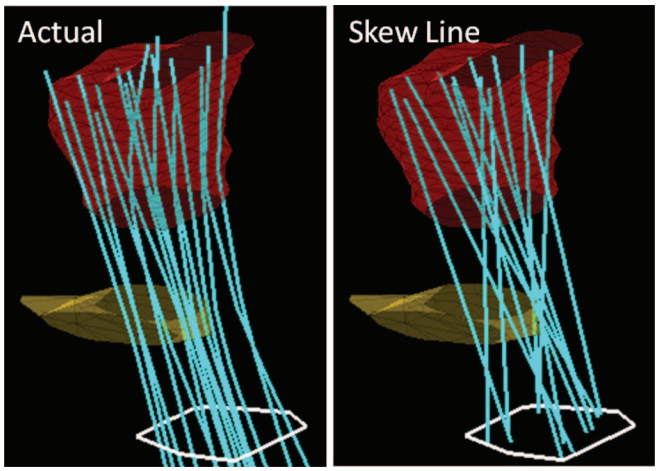

FIG. 1. Actual implant (left) and a computationally generated skew line configuration (right). Needles are shown as lines. The top structure is the prostate, and the middle structure is the penile bulb. The entry zone for needles is contoured in white at the bottom. The physician implant used 16 needles and intersected the penile bulb six times while the computed needle configuration used 13 needles and did not intersect the bulb. Both needle configurations met all dose objectives for the patient.

II. BACKGROUND

Integer programming is a central component of the needle planning system presented in this study. A brief overview of integer programming is given in this section. A detailed description of integer programming and common solution methods can be found in Nemhauser and Wolsey.[9]

A binary integer program (BIP) is an optimization model of the form,

$$\begin{array}{lll} & \text{minimize} & c^T x \\ \text{(BIP)} & \text{subject to:} & Ax \leq b \\ & \text{and} & x_i \in \{0,1\}, i = 1,\ldots,n, \end{array}$$

where the known parameters c, A, and b are $n \times 1$, $m \times n$, and $m \times 1$ matrices of real numbers, respectively, and x is an $n \times 1$ vector of decision variables (i.e., values which must be determined by an optimization algorithm) where each element of x can only take on the value 0 or 1. A feasible solution is an x that satisfies $Ax \leq b$ and $x_i \in \{0, 1\}$. The term $c^T x$ is called the objective function. The goal of an integer program solver is to find an optimal solution—a feasible solution with the lowest objective function value. A BIP is infeasible if there is exists no x that satisfies all the constraints.

Integer programs, including BIPs, can be solved using branch and bound (B&B) algorithms. B&B algorithms find an optimal solution by establishing a lower and upper bound on the optimal solution objective function value. The difference between the lower and upper bound is called the

optimality gap, or gap. B&B algorithms attempt to close gap by iteratively solving a large number of sub problems which are easier to solve than the original integer program. A feasible solution with objective function equal to the upper bound is guaranteed to be optimal when the gap is zero. However, it can take B&B algorithms a very long time to close the gap (i.e., establish an optimal solution). In these cases, it is useful to have termination criteria that stops a B&B algorithm and returns the best feasible solution found so far, assuming one has been found already. In many applications of integer programming these suboptimal, or not-provably-optimal, solutions are still of practical value.

III. METHOD AND MATERIALS

III.A. Needle configuration optimization

In this section, a system for computing skew line needle configurations is described. The system consists of a candidate needle generation component, a needle selection component, and a dose planning component. The candidate needle set is a large, virtual set of needles that is representative of the needles that are feasible for insertion. The needle selection component chooses a small subset of the candidate needles for insertion. The needle selection component should choose the needles in such a way as to be able to meet dose objectives during dose planning and such that the chosen needles do not intersect. The dose planning component is used to verify that the chosen needle configuration can meet dose objectives. Since integer programming is a central component of this system, we name it needle planning by integer program (NPIP). For reference, the notation used is given in Table I.

III.A.1. Candidate needle set generation

The candidate needle set generation component assumes it is possible for the user to define an entry zone where needles can be inserted into the body. Defining the entry zone in practice presents some challenges which are discussed in Sec. V.

TABLE I. NPIP terms.

Term	Description
E	Entry zone vertices
$\mathcal{E}$	Convex hull of E
C	Set of target contour points
T	Set of projected points above target
$\mathcal{T}$	Convex hull of T
N	Set of candidate needle
$\mathcal{N}$	Chosen set of needles to be inserted
P	Set of cover points
d_j	Coordinate of jth dwell position
δ	Needle coverage radius
x_k	Binary variable for $n_k \in N$
X	Set of pairs (k, ℓ) s.t. $n_k, n_\ell \in N$ collide
$K_i(\delta)$	Set of needles that cover $p_i \in P$ given δ
$I(\delta)$	Set of points that can be covered by N given δ

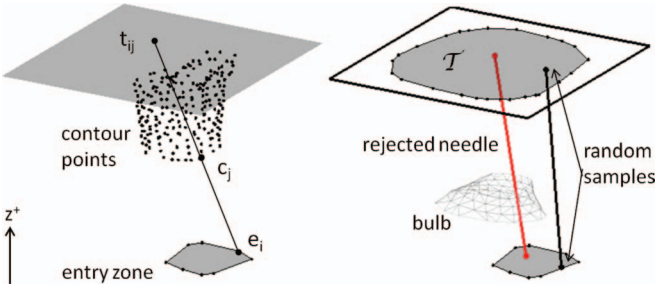

FIG. 2. A set of candidate needles was generated according to the anatomy of the patient. Given the vertices of an entry zone, E, and the contour points of the prostate, C, a set of points was computed, T, such that $t_{ij} \in T$ was the intersection of the line containing $e_i \in E$ and $c_j \in C$ with a plane perpendicular to the z-axis at the most superior slice of the target. The convex hull of T was called $\mathcal{T}$. A needle was generated by randomly sampling a point in $\mathcal{E}$, the convex hull of E, and in $\mathcal{T}$, and generating a line connecting them. Needles that intersected a healthy structure were removed.

Assume that the z-axis is parallel to the inferior-superior direction along the patient and let z^T be the z-coordinate of the most superior slice of the target. Let E be the set of vertices of the entry zone, $\mathcal{E}$ be the set of points in the convex hull of E, and C be the set of contour points of the target. The candidate needle set is generated according to the anatomy of the patient in four steps. (1) Compute $T = \{t_{ij} : t_{ij} = e_i + (\frac{z^T - e_i^z}{c_j^z - e_i^z})(c_j - e_i), \forall i \in E, \forall j \in C\}$. Here, e_i^z and c_j^z are the z-components of e_i and c_j, respectively, and t_{ij} is the intersection of the line going through e_i and c_j with a plane perpendicular to the z-axis at z^T. (2) Compute $\mathcal{T}$, the convex hull of T. (3) Generate a large number of needles by uniformly sampling a point in $\mathcal{E}$ and in $\mathcal{T}$ and creating a line between them. Each line represents a single needle. Sampling inside a convex polygon is discussed below. (4) Remove needles that do not intersect the target, remove needles that intersect a healthy structure before intersecting the target, and truncate needles that intersect a healthy structure after the prostate at a point before the intersection. Figure 2 shows a diagram of the terms used for generating candidate needle sets.

Uniform random sampling inside a convex polygon is described in Devroye.[10] First, the convex polygon is subdivided into triangles (i.e., a triangle mesh). Then, a triangle in the mesh is randomly selected with probability proportional to its area. Finally, a point is chosen from a uniform distribution inside the triangle.

III.A.2. Needle selection

Let the candidate needle set be denoted by N, and let $n_k \in N$ be a needle defined by the set of dwell positions that belong to it. The goal of the needle selection component is to find an $\mathcal{N} \subset N$ that (1) meets dose objectives, (2) is collision free, and (3) uses as few needles as possible. However, meeting dose objectives is a complicated constraint to enforce, and therefore, our needle selection component only requires that $\mathcal{N}$ have good spatial coverage of the target. Some mathematical formalism to these criteria is given and it is

shown that needle selection with these properties can be formulated as a BIP.

First the spatial coverage of needles is formalized. Assume that the target volume has been discretized into a grid of evenly spaced points, P. Usually, a point $p_i \in P$ is referred to as a "dose points" or "dose control points" because it is used to evaluate the dose delivered to an organ voxel. However, for this study the points are referred to as "cover points" to distinguish them from points used to control the dose distribution during dose planning. For a user-specified parameter, $\delta > 0$, n_k *covers* p_i if there exists a $d_j \in n_k$ such that $||p_i - d_j|| < \delta$, where d_j is a dwell position in n_k. Since δ defines the region that needles can cover, it is referred to as the needle coverage radius.

To achieve good spatial coverage of the target, it is desired that every point be covered by at least one needle in $\mathcal{N}$. However, some points may not be coverable by any needle in N, making this criterion impossible since $\mathcal{N} \subset N$. Instead, let $I(\delta)$ be the indices for the points which are coverable by at least one needle in the candidate set given δ: $I(\delta) = \{i : \exists n_k \in N$ that covers p_i given $\delta\}$, and $\mathcal{N}$ is said to give good spatial coverage of the target if there is a needle in $\mathcal{N}$ which covers every point in $I(\delta)$. Clearly for this criterion to be reasonable, $I(\delta)$ must contain the vast majority of points in P. Our experiments showed that in almost every case, every point in P was indexed in $I(\delta)$, and in cases which this was not true, $I(\delta)$ contained at least 98% of the points in P.

To avoid needle collisions, constraints on the selection process are added that restrict only one needle in a colliding pair to be chosen. Formally, let L_k be the line segment between the entry point and the most superior dwell position of n_k, and let n_k and n_ℓ collide if the minimum distance between L_k and L_ℓ is less than the diameter of a needle, γ. Define X to be the set of colliding pairs, (k, ℓ), between all the needles in N. If $\mathcal{N}$ is selected such that for every $(k, \ell) \in X$, only n_k or n_ℓ (but not both) can be chosen, then $\mathcal{N}$ is guaranteed to be collision free.

Minimizing the size of $\mathcal{N}$ subject to the coverage constraints defined by δ and the collision constraints defined by γ can be formulated as a BIP. Let x_k be an indicator variable for n_k with the following behavior:

$$x_k = \begin{cases} 1 & \text{if } n_k \text{ is chosen to be in the configuration,} \\ 0 & \text{otherwise,} \end{cases}$$

and let the parameter

$$K_i(\delta) = \{k : n_k \text{ covers } p_i \text{ given } \delta\}$$

be the set of needles that cover p_i given δ. Then needle selection, N(P, N, δ), is the following BIP:

$$\begin{aligned} & \text{minimize} && \sum_k x_k \\ \text{N}(P, N, \delta) \quad & \text{subject to:} && \sum_{k \in K_i(\delta)} x_k \geq 1, \quad \forall i \in I(\delta), && (1) \\ & && x_k + x_\ell \leq 1 \quad \forall (k, \ell) \in X, && (2) \\ & \text{and} && x_k \in \{0, 1\}, \quad \forall k. && (3) \end{aligned}$$

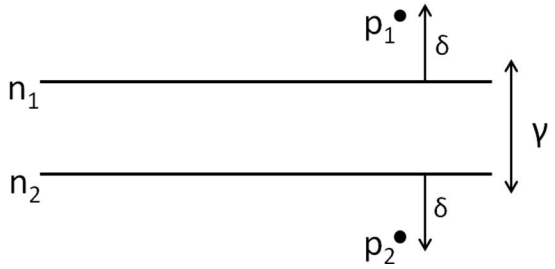

FIG. 3. Test case where coverage and collision-free requirement cannot both be met, even if every point can be covered by at least one needle in the candidate needle set. Here, n_1 can cover p_1 and n_2 can cover p_2. However, since they are less than γ apart, only one needle can be chosen. Thus, the problem is infeasible.

The objective function ensures that the fewest number of needles are chosen. Constraint 1 ensures that every point that can be covered is covered by at least one needle, constraint 2 ensures that only one needle in a colliding pair is chosen, and constraint 3 enforces the binary requirement on the definition of x_k.

Note that it is still possible for N(P, N, δ) to be infeasible, even if only the points in $I(\delta)$ are used for the coverage requirement, because it may be impossible to meet both the coverage and collision free requirement. A small test case in which this occurs is depicted in Fig. 3. Future work may be able to identify points that cannot be covered because of this restriction and exclude them from $I(\delta)$.

III.A.3. Dose planning

The primary objective of a needle configuration is to meet dose objectives. However, NPIP relaxes this requirement through a spatial coverage approximation defined by δ. Therefore, it is possible to choose δ such that dose objectives cannot be met by $\mathcal{N}$. For example, δ can be chosen large enough such that $|\mathcal{N}| = 1$, and a needle configuration with one needle will not meet reasonable dose objectives. Therefore, a dose planning tool is required to verify that $\mathcal{N}$ meets dose objectives.

Inverse planning by integer program (IPIP) (Ref. 11) was chosen as the dose planning tool for this system because it is guaranteed to meet all healthy-tissue sparing constraints while making target coverage as high as possible. These properties of IPIP allow needle configurations to be evaluated by a single metric, target coverage, without the need to interpret the relative value of competing dose objectives. Specifically, if IPIP produces a dose plan for a needle configuration that meets the target coverage requirement, then the needle configuration meets all dose objectives, and the needle configuration can be declared satisfactory. Otherwise, it is unsatisfactory.

III.B. Patient data sets

Data sets from 18 anonymized patients previously treated at our clinic were used for this study. These patients were chosen to have a wide range of prostate volumes ranging from 23 to 82 cm^3. The physician used a freehand technique to

implant 16 catheters into the prostate under transrectal ultrasound guidance. Plastic catheters were inserted transperineally by following the tip of the catheter from the apex of the prostate to the base of the prostate using ultrasound and a stepper. A Foley catheter was inserted to visualize the urethra.

Three-millimeter-thick CT slices were collected using a spiral CT. The implanted catheters, target (prostate), and the organs at risk (OAR) were contoured using Oncentra 3.2. The OAR included the rectum, bladder, urethra, and critical structures near the bulb. No margins were added. The structures near the penile bulb were contoured as a single organ and for the remainder of this paper will be referred to as the bulb. When segmenting the bladder and rectum, the outermost mucosa surface was contoured. The urethra was defined by the outer surface of the Foley catheter, and only the urethral volume within the prostate was contoured.

Contour slices with more than 15 points were reduced to 15 points. Reducing the number of contour points is a common feature in many dose planning systems. A visual inspection was made to ensure that the organ features were preserved. This reduction improved computational performance when generating cover points and checking for collisions between needles and organs.

A model of the entry zone was not available for this experiment because contouring it is not standard for HDR brachytherapy. Since an entry zone definition was critical for this study, the entry zone was taken to be the convex hull of the needle locations at a plane perpendicular to the z-axis taken 2 cm below the most inferior slice of the bulb, which was an estimation of the skin surface. A 5 mm margin was added to the entry zone so that the region would not be tight to the needle locations used. The needle locations in the plane were interpolated between the closest dwell positions to the plane. This entry zone definition ensured that NPIP needle configurations only utilized the space used by the physician. The entry zone area ranged from 7 to 13 cm^2.

III.C. Method evaluation

NPIP was used to compute needle configurations for each patient. For the candidate needle set generation component, the convex hull calculations were done using the MATLAB function, `convhull`, and convex hulls were subdivided into triangles using the MATLAB function, `delaunay`. The candidate needle sets were generated using 5000 random samples. This number of initial candidate needles was found to produce consistent results across trials. Dwell positions were generated along each needle from the entry zone to the needle tip in 5 mm increments. Needles intersected an organ if at any contour slice of that organ, the interpolated x-y position of that needle was contained in the slice. The tip of each needle was truncated at the most superior dwell position in the target.

A needle diameter of $\gamma = 1.7$ mm was used to check collisions. This is the diameter of the needles used in our clinic.

Cover points were generated for the target using a uniform grid with 5 mm spacing in the x-y direction and 3 mm spacing in the z-direction. Since the density of the final needle configuration was controlled by the user-parameter, δ, it was expected that for a given δ, large prostates would generate more needles than small prostates. To make the results from different-sized prostates more comparable, δ was always chosen relative to the radius of a sphere with equivalent prostate volume. For conciseness, all δ values in this study were stated as a percentage of this radius. For each patient candidate needle set, a needle configuration was computed for δ values ranging from 25% to 50% in increments of 5%. Initial tests with NPIP showed that this range of δ produced an interesting range of needle configuration sizes. Specifically choosing δ less than 25% produced needle configurations with more than 25 needles, which was too many to be clinically relevant, and choosing δ more than 50% had too few needles to meet dose objectives.

Instances of N(P, N, δ) were solved using MATLAB R2011a on a Lenova ThinkPad with an Intel i5-2410M processor and 4GB of RAM. The MATLAB interface for CPLEX 12.1 was used for the integer program optimization. There were six conditions to terminate the optimization process: (1) a provably optimal solution was found, (2) N(P, N, δ) was proven to be infeasible, (3) the optimization timer went over 10 min, (4) the memory usage exceeded 1 MB, (5) the number of branch and bound nodes exceeded 1000, or (6) the user aborted the process. In the third through sixth case, the feasible solution with the smallest objective function value was returned if one had been found already, and an error message was displayed otherwise. These conditions can be set in CPLEX using standard internal parameters. In practice, only a time limit needs to be specified for early termination. Other termination criteria were added for this study because there was no straightforward way to guarantee that the optimization solver would stop in 10 min, and more criteria were added to reduce the risk of running over time. These limitations are strictly due to the way CPLEX implements the time limit criterion. In a clinical deployment of this system, more extensive software should be written to ensure that the optimization solver stops when the timer expires.

A dose plan was generated for every computed needle configuration using IPIP. The IPIP parameters and dosimetric criteria used in this study were the same as in Siauw *et al.*,[11] except with the added restrictions that $V_{75}^{\text{Bulb}} \leq 1$ cm^3 and $V_{100}^{\text{Bulb}} = 0$ cm^3. This criteria was added to give some control over the dose to the bulb, which was not included in the original IPIP study. The dose objectives used in this study conform to the specifications given in the RTOG-0321 dosimetric protocol.[12] The requirements can be found in Table II. Only dwell positions inside the prostate were used for dose planning.

For each patient, the number of candidate needles, candidate needle set generation time, number of collision pairs, and collision calculation time was recorded. For each instance of N(P, N, δ), the number of points not included in $I(\delta)$, the time to construct the CPLEX optimization model, solve time, termination status, and the optimality gap at termination were recorded. The number of needles and compliance with dose objectives were recorded for every needle configuration

TABLE II. RTOG-0321 dosimetric protocol.

Index	Requirement
$V_{100}^{Prostate}$	≥90%
$V_{150}^{Prostate}$	≤45%
$V_{120}^{Urethra}$	≤0.1 cm^3
$V_{150}^{Urethra}$	=0 cm^3
V_{75}^{Rectum}	≤1 cm^3
V_{100}^{Rectum}	0 cm^3
$V_{75}^{Bladder}$	≤1 cm^3
$V_{100}^{Bladder}$	=0 cm^3
V_{75}^{Bulb}	≤1 cm^3
V_{100}^{Bulb}	=0 cm^3
V_{200}^{Body}	=0 cm^3

computed. To ensure the consistency of the results, the experiment was repeated five times.

For comparison, a dose plan was also computed from the physician implant using IPIP. The number of bulb punctures for each patient was also recorded.

IV. RESULTS

A needle configuration that used less needles than the physician, avoided the penile bulb, met all dose objectives, and was collision-free was computed for each patient. Results for each instance of N(P, N, δ) are summarized in Table III. Each table entry contains the average number of needles in N(P, N, δ) over the experiments, the average target coverage of the computed needle configurations over each experiment, and the number of instances that were feasible. The number of feasible instances is marked in bold if there were any infeasible instances. Note that the dose planning component, IPIP, was guaranteed to meet all dose objectives except target coverage. Therefore if target coverage was over 90%, the needle configuration met all dose objectives.

The number of needles and the ability to meet dose objectives decreased as the needle coverage radius, δ, increased. This was expected because a higher needle coverage radius allows each chosen needle to cover more volume, which requires fewer needles to cover every point. The table suggests that in practice, 35% or 40% could be chosen for the value of δ to ensure that the final needle configuration met dose objectives. For $\delta = 35\%$, N(P, N, δ) was sometimes (but rarely) infeasible, but when feasible, could always meet dose objectives. For $\delta = 40\%$, N(P, N, δ) was always feasible and on average, always met dose objectives. However, there were a few cases where target coverage was less than 90%. The likelihood of infeasibility did not appear to be related to the size of the prostate.

After needles were discarded due to collision with organs, the number of candidate needles ranged from 510 to 2599. Generally for each patient, the standard deviation of the number of candidate needles over the experiments was within 10% of the average number of needles. The runtime for generating the candidate needle set ranged from 17 to 55 s. Almost all the time generating candidate needle sets was spent checking for needle intersections with organs.

Collision checking needles found between 19 611 and 352 872 collision pairs, depending on the size of the candidate needle set. Collision checking took between 11 and 286 s.

There were 540 instances of N(P, N, δ) that were attempted: 18 patients × 6 δ-values × 5 experimental iterations. The number of cover points ranged from 463 to 1722. The number of points in $I(\delta)$ was less than the total number of

TABLE III. Table of results for N(P, N, δ). Each table entry contains (1) the average number of needles, (2) the average target coverage as a percentage of the target volume, and (3) the number of feasible instances of N(P,N,δ) over the NPIP experiments. Also included is the prostate size [cm^3] and entry zone size [cm^2]. Dose objectives could always be met by choosing $\delta = 35\%$ or 40%. These δ values corresponded to needle configurations with approximately 10–15 needles. Note IPIP guarantees healthy tissue sparing constraints. Therefore, if target coverage was met, then all dose objectives were met.

Px	Target	Entry zone	$\delta = 25\%$			$\delta = 30\%$			$\delta = 35\%$			$\delta = 40\%$			$\delta = 45\%$			$\delta = 50\%$		
1	23	11	23	99	5/5	15	99	5/5	12	97	5/5	9	95	5/5	8	93	5/5	7	90	5/5
2	26	9	19	99	5/5	13	98	5/5	10	96	5/5	8	93	5/5	6	86	5/5	6	81	5/5
3	27	12	20	99	5/5	14	98	5/5	10	93	5/5	8	91	5/5	6	84	5/5	5	75	5/5
4	28	10	25	99	5/5	17	98	5/5	12	95	5/5	9	94	5/5	8	90	5/5	6	85	5/5
5	28	13	22	100	5/5	14	99	5/5	10	97	5/5	8	94	5/5	7	89	5/5	6	84	5/5
6	30	7	–	–	**0/5**	18	98	**1/5**	15	97	**4/5**	11	95	5/5	9	93	5/5	8	87	5/5
7	34	9	–	–	**0/5**	20	98	**4/5**	15	95	5/5	11	93	5/5	9	91	5/5	7	81	5/5
8	34	9	22	100	5/5	16	99	5/5	11	98	5/5	9	94	5/5	8	91	5/5	6	87	5/5
9	34	12	20	99	5/5	15	98	5/5	11	96	5/5	8	96	5/5	7	89	5/5	6	83	5/5
10	38	8	33	99	**3/5**	22	98	**3/5**	15	97	5/5	11	95	5/5	9	91	5/5	8	87	5/5
11	40	12	24	100	5/5	16	99	5/5	12	97	5/5	9	96	5/5	7	90	5/5	6	89	5/5
12	42	9	32	99	**1/5**	20	98	5/5	14	97	5/5	11	95	5/5	9	92	5/5	7	92	5/5
13	43	10	29	96	5/5	18	94	5/5	13	92	5/5	10	90	5/5	8	86	5/5	7	86	5/5
14	48	12	24	96	5/5	17	95	5/5	13	94	5/5	10	91	5/5	8	87	5/5	7	81	5/5
15	49	11	–	–	**0/5**	19	97	5/5	14	96	**4/5**	11	95	5/5	9	92	5/5	8	88	5/5
16	61	10	33	99	**1/5**	20	97	**4/5**	15	96	**4/5**	12	95	5/5	10	92	5/5	7	87	5/5
17	69	13	25	97	5/5	16	96	5/5	12	95	5/5	10	93	5/5	8	91	5/5	7	88	5/5
18	85	11	27	97	5/5	18	96	5/5	13	95	5/5	10	92	5/5	8	91	5/5	7	86	5/5

cover points in 56/540 cases. The difference between the size of $I(\delta)$ and the size of P was between 1 and 9, and generally more points were removed when δ was small. The number of infeasible instances of N(P, N, δ) was 40/540. Infeasibility was more likely for smaller needle coverage radii, which was expected since it was harder to meet coverage when the needle coverage radius was small. However, small needle coverage radii were also associated with needle configurations which contained more needles than were required to meet dose objectives. The runtime of N(P, N, δ) ranged from 1 s to 2329 s, although there was an outlier that ran for 8809 s.

The total end-to-end runtime ranged from 31 s to 2968 s, excluding the case where N(P, N, δ) took 8809 s. The average runtime was 286 s. For a given patient, the total NPIP running time was approximately constant across δ values.

The physician implant could always meet dose objectives. The average number of intersections with the penile bulb was 5 with a standard deviation of 3. Every patient case had at least one bulb puncture. It is important to note that the bulb is not visible to the physician under ultrasound, but can be contoured later on for dose planning. In Fig. 1, the physician implant is shown as well as a 12 needle NPIP configuration for the same patient. The NPIP plans never intersected the penile bulb and met all dose objectives.

Given these results, needle configurations computed from NPIP have the potential to reduce side effects of HDR brachytherapy without compromising the high survival rate associated with this treatment modality. However, the execution of these needle configurations will probably require some form of robotic assistance. The use of robots has been been explored extensively for prostate permanent-seed implant (PPI) brachytherapy.[13–18] It is possible that this technology can be adapted to insert skew line needle configurations for HDR brachytherapy.

V. DISCUSSION

Needle configurations could be computed for each patient in our data set that avoided the penile bulb and met dose objectives. Since the bulb was punctured at least once by the physician in every patient case, and bulb puncturing may be related to side effects, there is potential for automatically generated needle configurations to reduce side effects of HDR brachytherapy. Robot-assisted brachytherapy is a framework that can utilize a needle planning system such as NPIP. However, some work is still required before HDR brachytherapy robots can become clinically relevant. Some of this work is discussed in this section.

Needle planning requires a definition of the entry zone where needles can be inserted into the body. The main challenge in defining the entry zone is that the patient is in supine position with legs closed during scanning, but legs open during needle insertion. Therefore, any entry zone definition made according to the CT scan would not be an accurate representation of the entry zone during the insertion procedure. To address this concern, the patient should either be scanned in a different position that could accommodate both the robot and the scanner, or the entry zone would need to be modified according to the change in position. Methodology to accomplish this task is beyond the scope of this paper.

NPIP requires a digitized anatomy set to compute a configuration of needles. However in the standard HDR brachytherapy workflow, the scan is taken after the needles have been inserted. This workflow inconsistency can be addressed by borrowing from the PPI brachytherapy workflow. In PPI brachytherapy, the patient is scanned and from the digitized anatomy set, a source configuration is computed and implanted by a physician. To incorporate NPIP into HDR brachytherapy, a similar approach can be taken. First, a scan is taken, then a needle configuration is computed, and finally is implanted by a physician or with the assistance of a robotic implant device. Another scan can then be taken to determine the needle locations for dose planning.

NPIP was designed to be used in conjunction with needle insertion robots. Care was taken in designing NPIP such that needle configurations computed from it could be executed by these robots. However, a study testing the implant feasibility of computationally generated needle configurations by robots should be done as a follow-up study. We suggest the following workflow for this future study: (1) scan a tissue phantom, (2) digitize the relevant anatomy, (3) compute a needle configuration with NPIP, (4) use a needle insertion robot to implant the needle configuration, (5) scan the phantom to verify the needle locations, (6) given the implanted needle configuration and patient anatomy, compute a dose plan for the patient, (7) deliver the dose plan in-silico, and (8) remove the needles.

VI. CONCLUSION

We have presented NPIP, a system for automatically generating skew line needle configurations that are patient-specific, collision-free, and avoid the penile bulb. We have shown that given the correct input parameters, NPIP can generate needle configurations which meet dose objectives and use as many or fewer needles than the current HDR brachytherapy workflow. Combined with robot assisted brachytherapy, this system has the potential to reduce side effects associated with treatment. A physical trial should be done to test the implant feasibility of NPIP needle configurations.

ACKNOWLEDGMENTS

The authors thank Judy Hoffman for the fruitful discussion at the inception of this project, and Ben Kehoe for his suggestion to normalize δ to prostate size.

[a] Author to whom correspondence should be addressed. Electronic mail: timmy.siauw@gmail.com

[1] F. Bachand, A.-G. Martin, L. Beaulieu, F. Harel, and É. Vigneault, "An eight-year experience of HDR brachytherapy boost for localized prostate cancer: Biopsy and PSA outcome," Int. J. Radiat. Oncol., Biol., Phys. **73**(3), 679–684 (2009).

[2] L. Eapen, C. Kayser, Y. Deshaies, G. Perry, Choan E, C. Morash, J. E. Cygler, D. Wilkins, and S. Dahrouge, "Correlating the degree of needle trauma during prostate brachytherapy and the development of acute urinary toxicity," Int. J. Radiat. Oncol., Biol., Phys. **59**(5), 1392–1394 (2004).

[3] P. W. McLaughlin, V. Narayana, A. Meirowitz, S. Troyer, P. L. Roberson, R. Gonda, Jr., H. Sandler, L. Marsh, T. Lawrence, and M. Kessler, "Vessel-sparing prostate radiotherapy: Dose limitation to critical erectile vascular

structures (internal pudendal artery and corpus cavernosum) defined by MRI," Int. J. Radiat. Oncol., Biol., Phys. **61**(1), 20–31 (2005).
[4]R. M. Munarriz, Q.-W. Robert Yan, A. Nehra, D. Udelson, and I. Goldstein, "Blunt trauma: The pathophysiology of hemodynamic injury leading to erectile dysfunction," J. Urol. (Baltimore) **153**, 1831–1840 (1995).
[5]C. Vargas, M. Ghilezan, M. Hollander, G. Gustafson, H. Korman, J. Gonzales, and A. Martinez, "A new model using number of needles and androgen deprivation to predict chronic urinary toxicity for high or low dose rate prostate brachytherapy," J. Urol. (Baltimore) **174**, 882–887 (2005).
[6]A. Graham Macdonald, M. Keyes, A. Kruk, G. Duncan, V. Moravan, and W. James Morris, "Predictive factors for erectile dysfunction in men with prostate cancer after brachytherapy: Is dose to the penile bulb important?," Int. J. Radiat. Oncol., Biol., Phys. **63**(1), 155–163 (2005).
[7]Y. Kim, I.-C. J. Hsu, and J. Pouliot, "Measurement of craniocaudal catheter displacement between fractions in computed tomography-based high dose rate brachytherapy of prostate cancer," J. Appl. Clin. Med. Phys. **8**(4), 1–13 (2007).
[8]J. Adam, M. Cunha, I.-C. Hsu, and J. Pouliot, "Dosimetric equivalence of nonstandard HDR brachytherapy catheter patterns," Med. Phys. **36**(1), 233–239 (2009).
[9]G. L. Nemhauser and L. A. Wolsey, *Integer and Combinatorial Optimization* (Wiley, New York, 1999).
[10]L. Devroye, *Non-Uniform Random Variate Generation* (Springer-Verlag, New York, 1986).
[11]T. Siauw, A. Cunha, A. Atamturk, I. Hsu, J. Pouliot, and K. Goldberg, "IPIP: A new approach to inverse planning for HDR brachytherapy by directly optimizing dosimetric indices," Med. Phys. **38**(7), 4045–4051 (2011).
[12]I-C. Hsu, K. Bae, K. Shinohara, J. Pouliot, J. Purdy, G. Ibbott, J. Speight, E. Vigneault, R. Ivker, and H. Sandler, "Phase II trial of combined high-dose-rate brachytherapy and external beam radiotherapy for adenocarcinoma of the prostate: Preliminary results of RTOG 0321," Int. J. Radiat. Oncol., Biol., Phys. **78**(3), 751–758 (2010).
[13]G. Fichtinger, J. P. Fiene, C. W. Kennedy, G. Kronreif, I. Iordachita, D. Y. Song, E. C. Burdette, and P. Kazanzides, "Robotic assistance for ultrasound-guided prostate brachytherapy," Med. Image Anal. **12**, 535–545 (2008).
[14]K. Cleary, V. Watson, D. Lindisch, R. H. Taylor, G. Fichtinger, C. S. White, S. Xu, J. Donlon, M. Taylor, A. Patriciu, D. Mazilu, and D. Stoianovici, "Precision placement of instruments for minimally invasive procedures using a 'needle driver' robot," Int. J. Med. Rob. Comput. Assist. Surg. **1**(2), 40–47 (2005).
[15]D. Stoianovici, D. Song, D. Petrisor, D. Ursu, D. Mazilu, M. Mutener, M. Schar, and A. Patriciu, "'MRI stealth' robot for prostate interventions," Minimally Invasive Ther. Allied Technol. **16**(4), 241–248 (2007).
[16]M. Muntener, A. Patriciu, D. Petrisor, M. Schär, D. Ursu, D. Y. Song, and D. Stoianovici, "Transperineal prostate intervention: Robot for fully automated MR imaging—System description and proof of principle in a canine model," Radiology **247**(2), 543–549 (2008).
[17]Y. Yu, T. Podder, Y. Zhang, W.-S. Ng, V. Misic, J. Sherman, L. Fu, D. Fuller, E. Messing, D. Rubens, J. Strang, and R. Brasacchio, "Robot-assisted prostate brachytherapy," In *Medical Image Computing and Compute-Assisted Intervention—MICCAI 2006* (Springer, New York, 2006), Vol. 4190.
[18]H. Su, M. Zervas, G. A. Cole, C. Furlong, and G. S. Fischer, "Real-time MRI-guided needle placement robot with integrated fiber optic force sensing," IEEE Int. Conf. Rob. Autom. **90**, 1583–1588 (2011).